HOLa: Zero-Shot HOI Detection with Low-Rank Decomposed VLM Feature Adaptation

Qinqian Lei¹ Bo Wang² Robby T. Tan^{1,3}
¹National University of Singapore ²University of Mississippi
³ASUS Intelligent Cloud Services (AICS)

qinqian.lei@u.nus.edu hawk.rsrch@gmail.com robby_tan@asus.com

Abstract

Zero-shot human-object interaction (HOI) detection remains a challenging task, particularly in generalizing to unseen actions. Existing methods address this challenge by tapping Vision-Language Models (VLMs) to access knowledge beyond the training data. However, they either struggle to distinguish actions involving the same object or demonstrate limited generalization to unseen classes. In this paper, we introduce HOLa (Zero-Shot HOI Detection with Low-Rank Decomposed VLM Feature Adaptation), a novel approach that both enhances generalization to unseen classes and improves action distinction. In training, HOLa decomposes VLM text features for given HOI classes via low-rank factorization, producing class-shared basis features and adaptable weights. These features and weights form a compact HOI representation that preserves shared information across classes, enhancing generalization to unseen classes. Subsequently, we refine action distinction by adapting weights for each HOI class and introducing human-object tokens to enrich visual interaction representations. To further distinguish unseen actions, we guide the weight adaptation with LLM-derived action regularization. Experimental results show that our method sets a new state-of-the-art across zero-shot HOI settings on HICO-DET, achieving an unseen-class mAP of 27.91 in the unseen-verb setting. Our code is available at https://github.com/ChelsieLei/HOLa.

1. Introduction

Human-object interaction (HOI) detection aims to identify humans and objects in images and predict their interactions, essential for many applications [7, 21, 23, 45, 52, 61, 63]. However, existing HOI detection struggles to generalize beyond seen classes, making zero-shot HOI detection a critical challenge [14, 30, 39]. Zero-shot HOI detection includes three primary settings: unseen composition, unseen

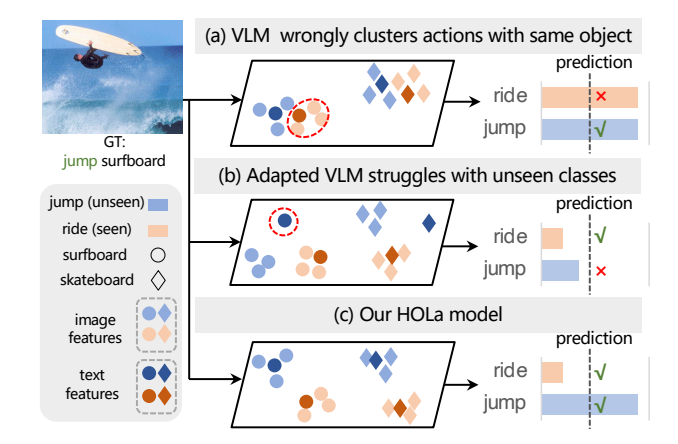


Figure 1. (a) HOI detection methods utilizing a frozen VLM feature space, struggle in distinguishing actions involving the same object [3, 30, 37, 39]. (b) Approaches that adapt VLMs to HOI tasks based on supervision from seen HOI classes, struggle to generalize effectively to unseen classes [22, 26]. (c) Our HOLa model decomposes VLM features into class-shared basis and adaptable weights, improving generalization to unseen HOI classes and enhancing action distinction.

object, and unseen action. In unseen composition HOI detection, actions and objects seen individually during training appear in novel combinations during testing, requiring models to recognize interactions beyond their training experience. This setting can be addressed via compositional learning strategies that independently classify objects and actions [14–16, 24]. Unseen object HOI detection focuses on detecting interactions involving objects not seen during training, which can be tackled with open-vocabulary object detectors [12, 38, 57]. However, since these approaches assume that all actions are observed during training, they cannot generalize to unseen actions.

A promising direction is leveraging Vision-Language Models (VLMs) to harness their broad knowledge beyond HOI training data. Existing methods following this approach fall into two main categories. The first maps HOI image features into the feature space of frozen VLMs [3, 29, 30, 37, 39], such as CLIP [42]. However, since VLMs are primarily trained on large-scale datasets focused on object recognition and description [42], they struggle to differentiate actions, especially those involving the same object. This limitation is critical in zero-shot HOI detection, where methods [3, 29, 30, 37, 39] depend on frozen VLMs to generalize to unseen classes without direct training supervision. Without explicitly refining VLM features to emphasize action-specific details, frozen VLMs lack the ability to distinguish actions involving the same object, as their representations primarily capture object semantics rather than nuanced action differences.

The second category [22, 26] adapts VLMs for HOI detection using prompt learning [18, 19, 44, 56, 65], reducing trainable parameters and computational costs. However, since training data provides annotations only for seen classes, these methods either do not explicitly leverage learned features for unseen classes [26] or lack sufficient supervision to guide generalization [22]. As a result, their adaptations fail to effectively generalize to unseen classes. Moreover, they adapt the VLM visual encoder without explicitly modeling interactions or rely on limited interaction patterns, which limits the effectiveness of action distinction.

To improve generalization to unseen classes while enhancing action distinction, we propose HOLa (Zero-Shot HOI Detection with Low-Rank Decomposed VLM Feature Adaptation), which introduces two key ideas: (1) improved generalization via low-rank decomposition of VLM features to capture class-shared information, and (2) enhanced action distinction through adapted decomposed VLM features with LLM-derived action regularization and human-object tokens that enrich interaction representations.

We first apply low-rank factorization to VLM text features derived from HOI class descriptions, decomposing them into basis features and adaptable weights. The basis features capture class-shared information, forming a foundation for HOI representation, while adaptable weights capture information unique to each HOI class. By combining basis features with adaptable weights, we construct a compact representation that retains shared knowledge across HOI classes, improving generalization to unseen classes.

However, distinguishing actions involving the same object remains challenging. The adaptable weights are derived from VLM text features, which struggle to encode finegrained action differences. To address this, we refine these weights through an adaptation process that enhances action distinction. However, since training data only supervise seen classes, direct weight adaptation struggles to distinguish unseen actions. To mitigate this, we introduce LLM-derived action regularization, which constrains the weight adaptation process to enhance generalization beyond seen actions. Additionally, we integrate human-object tokens to

encode spatial and appearance cues, further enriching visual interaction representations for action differentiation.

Fig. 1 illustrates the key differences between our approach and existing HOI detection methods. Fig. 1 (a) shows how existing methods rely on a frozen VLM feature space, clustering actions involving the same object together, which leads to ambiguities [3, 30, 37, 39]. Fig. 1 (b) depicts methods that adapt VLMs to HOI settings, where direct adaptation struggles to generalize to unseen classes effectively, as training data provides ground truths only for seen classes [22, 26]. In contrast, our method enhances action distinction and improves generalization to unseen classes through novel decomposed VLM feature adaptation. In summary, our contributions are:

- HOLa, a novel low-rank decomposed VLM feature adaptation method for zero-shot HOI detection, enhancing generalization to unseen classes, including unseen actions, while improving action distinction.
- A novel low-rank factorization approach to decompose and reconstruct VLM text features, generating a compact representation that captures class-shared information and improves generalization.
- Weight adaptation with LLM-derived action regularization and human-object tokens to refine interaction representation, both strengthening action distinction.

Extensive experiments on various zero-shot HOI settings demonstrate that our method achieves new state-of-the-art performance, reaching an unseen-class mAP of 27.91 in the unseen-verb setting on the HICO-DET dataset.

2. Related Work

Human-Object Interaction Detection HOI detection methods are broadly categorized into one-stage and two-stage approaches. One-stage methods predict all outputs simultaneously, including human and object bounding boxes, object categories, and interaction classes. Recent advancements leverage transformer architectures, achieving strong performance [6, 20, 36, 41, 47, 51, 55, 66]. In contrast, two-stage methods split HOI detection into object detection and HOI classification [11, 14, 24, 49, 58]. This separation allows each module to specialize, leading to a more efficient process [59]. Recent works have also integrated transformer architectures into two-stage designs, demonstrating promising results [40, 48, 60].

Zero-Shot HOI Detection Prior efforts in zero-shot HOI detection mainly address cases where action and object classes are seen individually but not in combination, using compositional learning strategies [14–16]. However, they struggle with unseen actions, as they require training representations for all actions and objects. A promising alternative is leveraging VLMs to incorporate external knowledge, especially for unseen classes. Several meth-

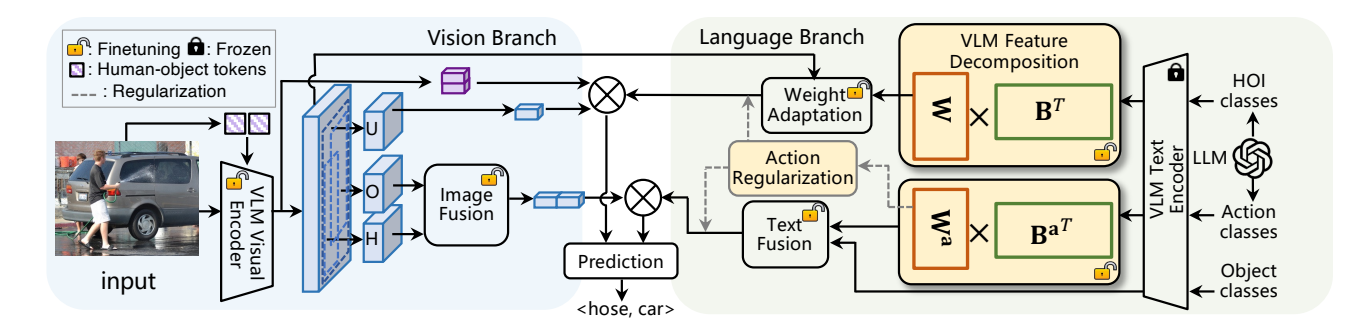


Figure 2. Overview of our HOLa. In the language branch, VLM text HOI features are decomposed into HOI basis features ${\bf B}$ and HOI weights ${\bf W}$. Similarly, action features are decomposed into action basis features ${\bf B}^a$ and action weights ${\bf W}^a$, where ${\bf B}^a$ is selected from ${\bf B}$. The weight adaptation updates ${\bf W}$ with LLM-derived action regularization ${\bf W}^a$, containing LLM-generated action information. The text fusion module combines action and object text features. In the vision branch, we adapt the VLM visual encoder with human-object tokens. Then we crop humans, objects, and HOI union regions from encoder output ("H, O, U" in the figure). The image fusion module then combines human and object features. The prediction combines vision and language branches.

ods align HOI visual features with frozen VLM text features [3, 30, 37, 39], but VLM features, trained primarily for object recognition [42], often fail to capture actions details, resulting in HOI classes involving the same object being clustered together despite differing actions. While our method also uses the frozen VLM text encoder, it avoids this issue by decomposing the features into class-shared basis and adaptable weights, enabling the model to refine action-specific differences and enhance action distinction.

Vision-Language Adaptations for HOI detection VLMs are widely used in tasks like image classification, semantic segmentation, etc, due to their strong image understanding capabilities (e.g. [1, 27, 28, 33, 34, 42]). Various adaptation techniques have been explored, including prompt tuning [18, 19, 44, 56, 64, 65] and learnable adapters [10, 17, 46, 54, 62]. In HOI detection, recent methods [22, 24, 26] adapt VLMs efficiently but struggle to generalize to unseen classes. Specifically, ADA-CM [24] performs poorly in the unseen-verb setting due to its memorybased design, which depends on ground-truth training data for each action, limiting generalization to unseen actions. Similarly, EZ-HOI [22] and CMMP [26] fail to generalize beyond seen classes, as their learnable prompts are finetuned solely on seen-class training data. This underscores the need for approaches that enhance generalization to unseen classes. Our method addresses this by introducing lowrank VLM feature decomposition and LLM-guided action regularization, avoiding reliance on memory-based adaptation (as in ADA-CM) and addressing the lack of generalization mechanism or supervision (as in CMMP and EZ-HOI).

3. Proposed Method

Our method follows the two-stage HOI detection framework, which uses an off-the-shelf object detector [4] and

focuses primarily on interaction classification [14, 16, 24, 26, 58, 59]. Let $\mathcal{A} = \{a_1, a_2, \cdots, a_{N_a}\}$ be the set of actions and $\mathcal{O} = \{o_1, o_2, \cdots, o_{N_o}\}$ be the set of objects. N is the total number of HOI classes. The HOI set consists of all given action-object pairs $\mathcal{C} = \{\text{hoi}_i = (a_{i_a}, o_{i_o}) \mid a_{i_a} \in \mathcal{A}, o_{i_o} \in \mathcal{O}\}$.

Zero-shot HOI detection requires HOI models to generalize to unseen classes during inference [30]. Let \mathcal{S} be the set of seen HOI classes, and let $\mathcal{U} = \{\text{hoi}_i \mid \text{hoi}_i \notin \mathcal{S}, \text{hoi}_i \in \mathcal{C}\}$ denote the set of unseen HOI classes. Our method follows standard zero-shot HOI settings, where the HOI class names of both seen and unseen classes are available during training. However, ground truth annotations (i.e., object bounding boxes, object labels, and their interaction labels) are provided only for seen classes and not for unseen ones [14, 15, 39, 50].

As shown in Fig. 2, our method consists of a language branch and a vision branch. The language branch decomposes VLM text features from HOI and action class names to capture class-shared information, enhancing generalization. These features are then refined through weight adaptation and text fusion modules respectively, incorporating LLM-derived action regularization to enhance action distinction. The vision branch utilizes a VLM visual encoder with our proposed human-object tokens to enhance interaction representation. Finally, the adapted language and vision features are fused for HOI prediction.

3.1. VLM Feature Decomposition and Adaptation

VLM Feature Decomposition Given HOI class names C, an LLM [9] generates detailed descriptions for each class, tapping its extensive knowledge beyond simple names. These descriptions are fed into the VLM text encoder, producing $\mathbf{F} = [\mathbf{f_1}, \mathbf{f_2}, \dots, \mathbf{f_N}]^{\top} \in \mathcal{R}^{N \times d}$, where d is the feature dimension. Each $\mathbf{f_i}$ corresponds to HOI class

 $\mathrm{hoi}_i = (a_{i_a}, o_{i_o})$ and carries richer, more nuanced HOI class information.

In feature decomposition, we aim to obtain basis features and corresponding weights. Let the learnable weights be $\mathbf{W} = [\boldsymbol{w_1}, \boldsymbol{w_2}, \dots, \boldsymbol{w_N}]^{\top} \in \mathcal{R}^{N \times m}$ and the learnable basis features be $\mathbf{B} = [\boldsymbol{b_1}, \boldsymbol{b_2}, \dots, \boldsymbol{b_m}] \in \mathcal{R}^{d \times m}$. The low-rank factorization of VLM text features \mathbf{F} is formulated as:

$$L_{\text{recon}}^{1} = \min_{\mathbf{W}, \mathbf{B}} ||\mathbf{F} - \mathbf{W}\mathbf{B}^{\top}||_{2}.$$
 (1)

Each $w_i \in \mathcal{R}^{m \times 1}$ in **W** corresponds to a specific HOI class hoi_i , while all $b_i \in \mathcal{R}^{d \times 1}$ in **B** are shared by all given HOI classes (i.e., both seen and unseen classes).

We apply L_1 loss to the weights **W** during low-rank factorization to encourage sparsity:

$$L_{\text{sparse}}^{1} = \min_{\boldsymbol{w_i}} \sum_{i=1}^{i=N} ||\boldsymbol{w_i}||_1.$$
 (2)

We impose an orthogonal constraint on **B** to enforce feature orthogonality, enabling it to capture disentangled features [43] shared across HOI classes:

$$L_{\text{ort}} = \min_{\boldsymbol{b_i}, \boldsymbol{b_j}} \sum_{i=1, i \neq j}^{i=m} \sum_{j=1}^{j=m} \boldsymbol{b_i}^{\top} \boldsymbol{b_j}.$$
 (3)

We reconstruct VLM text features using $\mathbf{W}\mathbf{B}^{\top}$ in a compact representation, highlighting shared features across HOIs and improving generalization to unseen classes.

Weight Adaptation Since VLM text features primarily focus on object information rather than actions [42], directly using the reconstructed features \mathbf{WB}^{\top} for HOI prediction is suboptimal, as it struggles to distinguish actions involving the same object. To address this, we introduce a text adapter to refine \mathbf{WB}^{\top} specifically for HOI tasks.

First, we introduce down projection layers at the text adapter input and up projection layers at its output to reduce feature dimensions for efficient adaptation. The input $\mathbf{W}\overline{\mathbf{B}}^{\mathsf{T}}$, where $\overline{\mathbf{B}}$ represents the fixed basis features without gradients, first passes through a self-attention module. It then enters a cross-attention mechanism, where the self-attention output serves as the query, and the key and value are derived from the input image features f_{img} to integrate visual context. Finally, a residual connection adds the input $\mathbf{W}\overline{\mathbf{B}}^{\mathsf{T}}$ back to the output, refining the adaptation while preserving input information. The adapted weights \mathbf{W} , when multiplied by $\overline{\mathbf{B}}^{\mathsf{T}}$, yield the reconstructed HOI text features, which we denote as the adapted features $\hat{\mathbf{F}}$.

Keeping $\overline{\mathbf{B}}$ unchanged is essential for preserving shared information across HOI classes from the VLM. Thus, the text adapter fine-tunes only the weights \mathbf{W} for each HOI class, optimizing them with the action classification loss

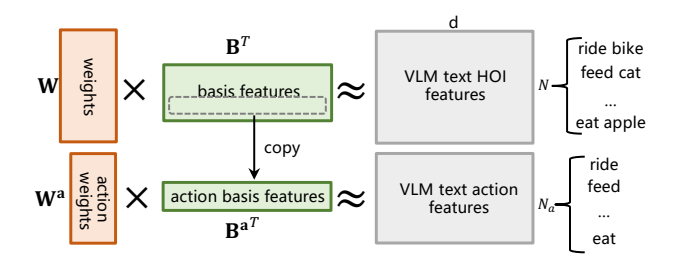


Figure 3. VLM text feature decomposition illustration. We first decompose HOI features into basis features ${\bf B}$ and weights ${\bf W}$. Then we obtain action-related basis features from ${\bf B}$, which can be used to reconstruct the action features.

in Eq. (8) to enhance action distinction while maintaining shared HOI knowledge.

3.2. Language Branch

As shown in Fig. 2, our language branch processes both HOI class names and separate action and object names. HOI text features, derived from HOI class names, capture richer interaction information, while weight adaptation enhances action distinction. However, its dependence on seenclass training data limits generalization. To address this, we introduce LLM-derived action regularization to guide adaptation, improving unseen action distinction. We then fuse the action text features with object text features for a more robust representation.

LLM-Derived Action Regularization Our idea is to leverage LLM-derived action regularization to constrain adaptable weights during adaptation, preventing an over-reliance on seen-class information. First, we utilize an LLM to generate detailed action descriptions for each action class in \mathcal{A} . These descriptions are then encoded into action text features using a VLM text encoder, producing $\mathbf{F}^a = [f_1^a, f_2^a, \cdots, f_{N_a}^a]^\top \in \mathcal{R}^{N_a \times d}$. Next, \mathbf{F}^a is decomposed into weights $\mathbf{W}^a \in \mathcal{R}^{N_a \times k}$ and basis features $\mathbf{B}^a \in \mathcal{R}^{d \times k}$, with the factorization process formulated as:

$$L_{\text{recon}}^2 = \min_{\mathbf{W}^a \mathbf{B}^a} ||\mathbf{F}^a - \mathbf{W}^a \mathbf{B}^{a \top}||_2, \tag{4}$$

where $k \ll \min(d, N_a)$. The decomposition includes a sparsity constraint on \mathbf{W}^a , expressed as: $L_{\mathrm{sparse}}^2 = \min_{\boldsymbol{w}_i^a} \sum_{i=1}^{i=N_a} \|\boldsymbol{w}_i^a\|_1$.

The action basis \mathbf{B}^a is randomly sampled from \mathbf{B} at initialization and shared by both HOI and action reconstruction, so the action reconstruction enforces action cues in \mathbf{B}^a . We denote b_i as the *i*-th row of the matrix \mathbf{B} that also belongs to the subset \mathbf{B}^a , and define the index set $\mathcal{I} = \{i \mid b_i \in \mathbf{B}^a\}$. Since \mathbf{W}^a encodes nuanced action information derived from action descriptions for both seen and unseen classes, we use it to regularize a matching subset of the adapted HOI weights \mathbf{W} . Concretely, we extract

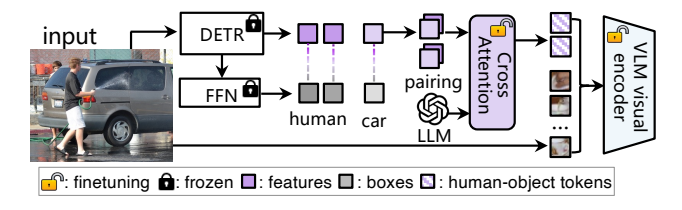


Figure 4. Human-object token illustration in the vision branch.

the subset $\mathbf{W}_{\mathrm{ar}} = \{\hat{\boldsymbol{w}}_i' \mid i \in \mathcal{I}\}$, where $\hat{\boldsymbol{w}}_i'$ denotes the *i*-th column of the adapted matrix \mathbf{W} . Finally, we align \mathbf{W}_{ar} with \mathbf{W}^a by minimizing their KL divergence:

$$L_{\text{act}}^{1} = \min D_{\text{KL}}[\mathbf{W_{ar}} \parallel \mathbf{W}^{a}], \tag{5}$$

where $D_{\rm KL}$ represents the KL divergence.

This approach encourages the adapted action-related subset W_{ar} to align with the weight distributions of W^a , integrating action knowledge from LLM-derived action regularization. As a result, the adaptation of W_{ar} is no longer limited to seen-class training data but is also guided by W^a , which extracts generalizable action information from LLM-generated descriptions. This enhances action distinction, particularly for unseen classes.

Text Fusion While HOI text features capture overall human-object interactions, individual action and object text features provide finer details specific to each component. Fusing action and object text features combines these details, enriching the HOI representation with more precise object and action information.

Specifically, the input to the text fusion module is the concatenated action and object features: $\operatorname{concat}(\mathbf{W}^a\overline{\mathbf{B}}^{a\top},\mathbf{F}^o)$, where the action feature is reconstructed from action basis features, $\overline{\mathbf{B}}^a$, and action weights \mathbf{W}^a . The object features \mathbf{F}^o are obtained through VLM text encoders with a template input "a photo of $\langle \operatorname{object} \rangle$ ". To reduce computational cost, we incorporate down and up projection layers. The input features then pass through a self-attention module, integrating action and object information. Finally, a residual connection adds the input back to the output to retain input information. We refer to the text fusion output as the adapted features $\hat{\mathbf{F}}^{ao}$.

We design adapted action weights \mathbf{W}^a to enhance action distinction while leveraging object information to enrich interaction understanding, capturing variations in actions across different object contexts (e.g., riding a bus vs. riding an elephant). We apply LLM-derived action regularization during the adaptation of \mathbf{W}^a to improve unseen action distinction:

$$L_{\text{act}}^2 = \min D_{\text{KL}}[\text{ adapted } \mathbf{W}^a \parallel \mathbf{W}^a]. \tag{6}$$

3.3. Vision Branch

To enhance interaction representation and action distinction, we introduce human-object tokens in the vision branch, as shown in Fig. 4. We utilize a pretrained DETR model [4] for object detection, identifying all detected humans (h_i) and objects (o_j) , where i and j denote the indices of detected human and object instances, respectively.

For each detection, we extract human and object features from the DETR decoder, denoted as f_{h_i} and f_{o_j} . We generate all possible human-object feature pairs, represented as (f_{h_i}, f_{o_j}) . We compute spatial features from paired human-object bounding boxes, denoted as $f_{\text{ho}ij}^{\text{spatial}}$, which facilitate interaction recognition. The human-object tokens are computed: $T_{\text{ho}ij} = \frac{f_{h_i} + f_{o_j}}{2} + f_{\text{ho}ij}^{\text{spatial}}$, which integrates both appearance and spatial cues to enhance interaction representation for a human-object feature pair (f_{h_i}, f_{o_j}) . The human-object token set is T_{ho} where $T_{\text{ho}} = \{T_{\text{ho}ij} \mid 1 \leq i \leq n_h, 1 \leq j \leq n_o\}$.

After generating human-object tokens $T_{\mathrm{ho}_{ij}}$, we use an LLM to generate interaction prior knowledge features, which are combined with $T_{\mathrm{ho}_{ij}}$ as the output. These human-object tokens, along with image patches, are then fed into the visual encoder, which outputs the adapted human-object tokens $\hat{T}_{\mathrm{ho}_{ij}}$ and a global image feature map $f_{\mathrm{img}}^{\mathrm{glb}}$. We consequently obtain human, object and human-object union visual features, denoted as f_{img}^h , f_{img}^o , f_{img}^u from $f_{\mathrm{img}}^{\mathrm{glb}}$. The image fusion module fuses human and object visual features, denoted as $f_{\mathrm{img}}^{\mathrm{ho}}$ enhancing interaction representation. Additional details are provided in the supplementary.

3.4. Training and Inference

Training We can calculate the final action prediction s_a using:

$$s_{a} = \gamma_{1} * (\operatorname{sim}(f_{\operatorname{img}}^{u}, \hat{\mathbf{F}}) + \operatorname{sim}(\hat{T}_{\operatorname{ho}}, \hat{\mathbf{F}})) * l_{u}^{R} +$$

$$\gamma_{2} * \operatorname{sim}(f_{\operatorname{img}}^{\operatorname{ho}}, \hat{\mathbf{F}}^{\operatorname{ao}}) * l_{ao}^{R},$$

$$(7)$$

where l_u^R is the action class label corresponding to the adapted HOI features $\hat{\mathbf{F}}$ and l_{ao}^R is the action class label corresponding to $\hat{\mathbf{F}}^{\mathbf{ao}}$. One action class can be associated with multiple HOI classes. If an action a_{i_a} corresponds to q HOI classes, the labels related to a_{i_a} in l_u^R and l_{ao}^R are scaled by a normalization weight of 1/q. $\sin(\cdot \mid \cdot)$ indicates the cosine similarity. γ_1, γ_2 are hyper-parameters. We compute the classification loss L_{cls} for action classification:

$$L_{\rm cls} = {\rm FL}(s_a, s_{\rm GT}),$$
 (8)

where FL represents focal loss [32] and $s_{\rm GT}$ represents the ground-truth action label. We also apply a semantic loss $L_{\rm sem}$ to facilitate the action distinction (detailed in the supplementary).

Apart from supervision using HOI training data, we also include the following VLM feature decomposition constraints during training:

$$L_{\text{fd}} = \beta_1 (L_{\text{recon}}^1 + L_{\text{recon}}^2) + \beta_2 (L_{\text{sparse}}^1 + L_{\text{sparse}}^2) + \beta_3 L_{\text{ort}} + \beta_4 (L_{\text{act}}^1 + L_{\text{act}}^2).$$
(9)

The final loss is obtained by: $L_{\text{total}} = L_{\text{cls}} + \alpha L_{\text{sem}} + L_{\text{fd}}$.

Generalization via Feature Decomposition $L_{\rm fd}$ continuously update the basis ${\bf B}$ in training by reconstructing the fixed VLM features and it serves as a regularizer to preserve unseen-class information in ${\bf B}$. Specifically, if ${\bf B}$ is overly influenced by the classification loss $L_{\rm cls}$ and overfits to seen classes, its reconstruction error on the unseen classes of ${\bf F}$ increases, and then $L_{\rm fd}$ penalizes it accordingly. In contrast, direct adaptation guided by $L_{\rm cls}$ alone loses unseen-class information in ${\bf F}$ and overfits to seen classes. By decomposing ${\bf F}$ into ${\bf WB}^{\top}$, each feature is reconstructed as a mixture of seen and unseen classes. The class-shared basis ${\bf B}$ enforces the adaptation to incorporate unseen information, thus preserving generalizable knowledge.

Inference At the test stage, we use an off-the-shelf detector [4] for human and object detection and obtain human bounding boxes b_h , object bounding boxes b_o and their related classification score s_h , s_o . From Eq.(13), we can obtain the action classification score s_a . Finally, the HOI score for each human-object pair is computed as follows:

$$s_{h,o}^{a} = (s_h * s_o)^{\tau} * \sigma(s_a),$$
 (10)

where $\sigma(\cdot)$ denotes sigmoid function, τ is a hyperparameter.

4. Experiments

Dataset We evaluate our method on the HICO-DET dataset [5], a widely used benchmark for human-object interaction detection. Following prior works [3, 30, 37, 39], we assess performance under four zero-shot HOI detection settings: unseen verb (UV), non-rare first unseen composition (NF-UC), rare first unseen composition (RF-UC), and unseen object (UO). Additionally, we provide quantitative evaluations under the fully supervised setting on the HICO-DET and V-COCO datasets in the supplementary materials, where our method also achieves competitive results.

Evaluation Metrics Following established evaluation protocols for HOI detection, we evaluate our model using mean average precision (mAP) [24, 30, 39, 66]. To provide a more balanced assessment, we also report the harmonic mean (HM) metric [26], which measures performance across both seen and unseen HOI classes, preventing the evaluation from being skewed by the larger number of seen classes.

Method	HM	Unseen	Seen	Full
ADA-CM [24] (ICCV'23)	21.67	17.33	28.92	27.29
GEN-VLKT [30] (CVPR'22)	24.76	20.96	30.23	28.74
HOICLIP [39] (CVPR'23)	27.69	24.30	32.19	31.09
UniHOI [3] (NeurIPS'23)	26.62	22.18	33.29	30.87
LogicHOI [29] (NeurIPS'23)	27.75	24.57	31.88	30.77
CLIP4HOI [37] (NeurIPS'23)	28.35	26.02	31.14	30.42
CMMP [26] (ECCV'24)	<u>29.13</u>	<u>26.23</u>	32.75	31.84
EZ-HOI [22] (NeurIPS'24)	28.69	25.10	33.49	32.32
Ours (HOLa)	31.09	27.91	35.09	34.09

Table 1. Quantitative comparison of zero-shot HOI detection with state-of-the-art methods in the Unseen-Verb (UV) setting on HICO-DET. HM denotes the harmonic mean.

Method	HM	Unseen	Seen	Full
GEN-VLKT [30] (CVPR'22)	24.19	25.05	23.38	23.71
HOICLIP [39] (CVPR'23)	27.22	26.39	28.10	27.75
ADA-CM [24] (ICCV'23)	31.75	32.41	31.13	31.39
UniHOI [3] (NeurIPS'23)	26.21	26.89	25.57	25.96
LogicHOI [29] (NeurIPS'23)	27.34	26.84	27.86	27.95
CLIP4HOI [37] (NeurIPS'23)	29.77	31.44	28.26	28.90
CMMP [26] (ECCV'24)	30.85	32.09	29.71	30.18
EZ-HOI [22] (NeurIPS'24)	32.03	<u>33.66</u>	<u>30.55</u>	31.17
Ours (HOLa)	33.35	35.25	31.64	32.36

Table 2. Quantitative comparison of zero-shot HOI detection with state-of-the-art methods in Non-Rare First Unseen-Composition (NF-UC) setting on HICO-DET. HM denotes the harmonic mean.

Implementation Details For object detection, we use a pretrained DETR model [4] with a ResNet50 [13] backbone, fine-tuned on HICO-DET, following existing zero-shot two-stage HOI detection methods [2, 14, 24]. We set m=71, k=35 for feature decomposition, with a VLM feature dimension of d=512. In Eq.(13), we use $\gamma_1=2.66, \gamma_2=2.66$. In Eq.(9), we set $\beta_1=0.1, \beta_2=0.1, \beta_3=0.001, \beta_4=50$. For training loss calculation $L_{\rm total}$, we assign $\alpha=80$. The temperature τ in Eq.(13) is set to 1 during training and 2.8 during inference [58, 59]. To ensure a fair comparison with baseline methods leveraging VLMs, we use the CLIP model with the same ViT-B backbone [8]. More details can be found in the supplementary.

4.1. Zero-Shot HOI Detection Evaluation

Unseen-Verb Setting Table 1 shows that our method outperforms all existing approaches, establishing a new state-of-the-art across every metric. For unseen classes, our method achieves 27.91 mAP (+6.40%) and an HM score of 31.09 (+6.73%), surpassing the previous best result from CMMP [26]. Our improved performance stems from our proposed modules, where low-rank factorization extracts class-shared basis features, allowing unseen classes to be effectively represented. Additionally, LLM-derived regularization mitigates reliance on training data supervision,

Method	HM	Unseen	Seen	Full
GEN-VLKT [30] (CVPR'22)	25.91	21.36	32.91	30.56
HOICLIP [39] (CVPR'23)	29.47	25.53	28.47	32.99
ADA-CM [24] (ICCV'23)	30.62	27.63	34.35	33.01
UniHOI [3] (NeurIPS'23)	27.54	23.41	33.45	31.97
LogicHOI [29] (NeurIPS'23)	29.79	25.97	34.93	33.17
CLIP4HOI [37] (NeurIPS'23)	31.59	28.47	35.48	34.08
CMMP [26] (ECCV'24)	31.07	<u>29.45</u>	32.87	32.18
EZ-HOI [22] (NeurIPS'24)	<u>31.38</u>	29.02	34.15	33.13
Ours (HOLa)	32.69	30.61	35.08	34.19

Table 3. Quantitative comparison of zero-shot HOI detection with state-of-the-art methods in Rare First Unseen-Composition (RF-UC) setting on HICO-DET. HM denotes the harmonic mean.

Method	HM	Unseen	Seen	Full
GEN-VLKT [30] (CVPR'22)	15.42	10.51	28.92	25.63
HOICLIP [39] (CVPR'23)	21.28	16.20	30.99	28.53
UniHOI [3] (NeurIPS'23)	18.83	13.67	30.27	27.52
LogicHOI [29] (NeurIPS'23)	20.66	15.64	30.42	28.23
ADA-CM [24] (ICCV'23)	32.40	33.26	31.59	31.87
CLIP4HOI [37] (NeurIPS'23)	32.25	31.79	32.73	32.58
CMMP [26] (ECCV'24)	32.40	33.76	31.15	31.59
EZ-HOI [22] (NeurIPS'24)	32.66	33.28	32.06	32.27
Ours (HOLa)	34.65	36.45	33.02	33.59

Table 4. Quantitative comparison of zero-shot HOI detection with state-of-the-art methods in Unseen-Object (UO) setting on HICO-DET. HM denotes the harmonic mean.

leading to improved unseen action distinction.

Unseen-Composition Setting The unseen composition setting includes two scenarios: non-rare first (NF-UC) and rare first (RF-UC). In the NF-UC setting (Table 2), where common HOI classes are unseen, our method achieves the highest performance across all metrics, demonstrating its strong generalization ability. Our method surpasses the previous state-of-the-art by 1.59 mAP on unseen classes while achieving 31.64 mAP on seen classes. In the RF-UC setting (Table 3), where rare HOI classes are unseen, our method outperforms all existing approaches, exceeding the previous best (CMMP [26]) by 1.59 mAP on unseen classes. Our method also achieves the best harmonic mean (HM) and full metric scores, ensuring a more balanced seen-unseen performance. While CLIP4HOI [37] scores 0.4 mAP higher on seen classes, our method demonstrates stronger generalization, outperforming it by 2.14 mAP on unseen classes.

Unseen-Object Setting Table 4 presents the unseen-object (UO) setting performance comparison. For a fair comparison, we focus on two-stage methods [22, 24, 26, 37], all using the same object detector [4]. Our method outperforms all baselines across all metrics, achieving a 2.69 mAP gain on unseen classes. This underscores our model's superior

			Txt. Fusion		Unseen	Seen	Full
$\overline{}$	×	×	×	×	23.58	31.55	30.43
\checkmark	×	×	×	×	25.76	31.35	30.57
\checkmark	\checkmark	\times	×	×	25.47	33.59	32.46
\checkmark	\checkmark	\checkmark	×	×	26.69	33.28	32.36
\checkmark	\checkmark	\checkmark	\checkmark	×	27.19	33.55	32.66
\checkmark	\checkmark	\checkmark	\checkmark	\checkmark	27.91	35.09	34.09

Table 5. Ablation study for main components of our method in the unseen-verb zero-shot setting. "Feat. Dec." denotes feature decomposition, "Wgt. Adapt." denotes the weights adaptation, "LLM Reg." denotes the LLM-derived action regularization, and "Txt. Fusion" denotes the text fusion module. "HO Token" denotes the human-object tokens in vision branch.

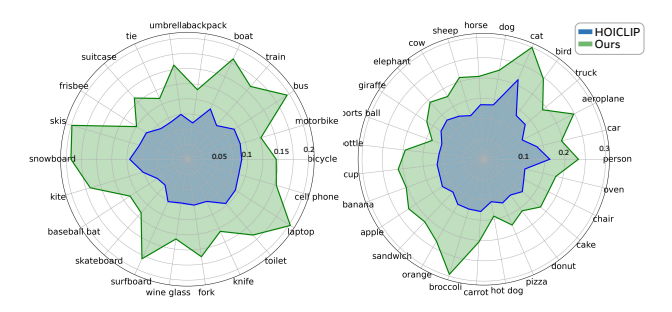


Figure 5. Action dissimilarity comparison. The action dissimilarity (AD) of our reconstructed text features $\hat{\mathbf{F}}$ (green) is compared to that of the original VLM text features used by HOICLIP [39] (blue). Higher AD values indicate better differentiation between actions involving the same object.

generalization to unseen object classes.

4.2. Ablation Studies

Major Module Evaluation Table 5 presents an ablation study on key modules under the unseen-verb zero-shot setting. The baseline (Row 1) excludes our proposed modules. To improve generalization, we introduce VLM feature decomposition and LLM-derived action regularization. VLM feature decomposition (Row 2) increases unseen mAP by 2.18 by reconstructing VLM features into basis features and weights, emphasizing class-shared information. LLM-derived action regularization (Row 4) further improves unseen action distinction, adding a 1.22 mAP gain compared to weight adaptation without regularization (Row 3).

To refine action distinction, we introduce weight adaptation with LLM-derived action regularization and humanobject tokens in the vision branch. The adaptable weights, optimized via action classification loss, improve seen-class performance by 2.24 mAP but slightly reduce unseen-class performance by 0.29 mAP due to reliance on seen-class ground truths. LLM-derived action regularization mitigates this, increasing unseen mAP by 1.22. Lastly, human-object

\mathbf{W}	В	Unseen 22.95	Seen	Full	\mathbf{W}	В	Unseen	Seen	Full
\mathbf{W}	В	22.95	30.30	29.27	\mathbf{W}	$\overline{\mathbf{B}}$	25.47	33.59	32.46

Table 6. Ablation study for weights and basis features optimization in the unseen-verb zero-shot setting. \mathbf{X} means applying classification loss $L_{\rm cls}$ and feature decomposition loss $L_{\rm fd}$ in training to update \mathbf{X} . $\overline{\mathbf{X}}$ denotes applying only $L_{\rm fd}$. $\mathbf{X} \in \{\mathbf{W}, \mathbf{B}\}$.

tokens enhance interaction representation in the visual encoder, improving full mAP by 1.43.

To visualize enhanced action distinction, we compare our reconstructed HOI text features, derived from basis features and adapted weights, with the original VLM text features used by HOICLIP [39]. We define action dissimilarity for an object o_{i_o} and its associated action set \mathcal{A}_{i_o} as: $AD_{i_o} = \frac{1}{|\mathcal{A}_{i_o}|} \sum_{i,j \in \mathcal{A}_{i_o}, i \neq j} (1 - \boldsymbol{f}_i^{\top} \boldsymbol{f}_j)$ where $|\mathcal{A}_{i_o}|$ is the number of actions in \mathcal{A}_{i_o} , and $\boldsymbol{f}_i, \boldsymbol{f}_j \in \mathcal{R}^{d*1}$ are the text features of HOI classes hoi_i and hoi_j . Fig. 5 plots AD_{i_o} for different objects, showing that our reconstructed text features achieve higher action dissimilarity, leading to better differentiation between actions involving the same object.

VLM Feature Decomposition and Adaptation Table 15 presents an ablation study on VLM feature decomposition and adaptation. To evaluate their effectiveness in isolation, we add only these two components to the baseline method (Row 3 in Table 5), excluding other proposed modules. On the left, applying classification loss $L_{\rm cls}$ to both weights and basis features negatively affects both components during training. On the right, $L_{\rm cls}$ is applied only to weights, while $L_{\rm fd}$ is used for both (W, $\overline{\rm B}$), leading to a 3.29 mAP gain on seen classes and 2.52 mAP on unseen classes over the baseline. These results show that updating both basis features and weights with $L_{\rm cls}$ reduces the effectiveness of class-shared information extraction, leading to a large performance drop.

LLM Description We integrate LLM-generated descriptions for HOI and action classes in the language branch. Table 7 presents an ablation study on their impact. Without LLM descriptions, we use a fixed template: "a person \(\text{ acting } \) a/an \(\text{ object } \)", the baseline unseen-class performance is 30.06 mAP (Row 1 in the Table 7). Using our proposed method without the LLM (Row 2) improves unseen-class mAP by 4.60 over the baseline. In contrast, adding LLM descriptions alone to the baseline provides only a 0.37 mAP boost, showing minimal standalone impact (Row 3). With both our method and LLM descriptions (last row), unseen-class performance improves by 4.33 mAP compared to using LLM descriptions alone, demonstrating that our method's effectiveness comes from its design rather than LLM reliance. Additional ablation studies for LLM description are provided in the supplementary.

Ours	LLM Description	Unseen	Seen	Full
×	×	21.05	31.53	30.06
\checkmark	×	25.65	33.86	32.71
×	✓	23.58	31.55	30.43
\checkmark	\checkmark	27.91	35.09	34.09

Table 7. Ablation study for LLM descriptions in the language branch. "Ours" refers to our proposed HOLa modules.



Figure 6. Visualization of unseen HOI predictions in the unseenverb setting on HICO-DET.

4.3. Qualitative Results

Fig. 6 visualizes HOLa's predictions in the unseen-verb setting of HICO-DET. Our method successfully detects unseen actions like "hose", "toast" and "swing", showcasing strong generalization to unseen HOI classes. This success stems from our low-rank decomposed feature adaptation, which captures class-shared information, while LLM-derived action regularization guides weight adaptation, for enhanced action distinction, especially for unseen actions.

5. Conclusion

We introduced HOLa, a novel Low-Rank Decomposed VLM Feature Adaptation method for zero-shot HOI detection, boosting generalization to unseen classes and action distinction. HOLa employs low-rank factorization to decompose VLM text features into class-shared basis features and adaptable weights. The weights adapt each HOI class to improve action distinction, while the basis features, combined with weights, create a compact representation that preserves class-shared information, enhancing generalization. To overcome the limitations of adapting weights solely from training data, we introduce LLM-derived action regularization to guide adaptation. Additionally, human-object tokens refine visual interaction representation, further improving action distinction. HOLa achieves 27.91 mAP in the unseen-verb setting, establishing a new state-of-the-art in zero-shot HOI detection.

References

- [1] Jean-Baptiste Alayrac, Jeff Donahue, Pauline Luc, Antoine Miech, Iain Barr, Yana Hasson, Karel Lenc, Arthur Mensch, Katherine Millican, Malcolm Reynolds, et al. Flamingo: a visual language model for few-shot learning. *Advances in Neural Information Processing Systems*, 35:23716–23736, 2022. 3
- [2] Ankan Bansal, Sai Saketh Rambhatla, Abhinav Shrivastava, and Rama Chellappa. Detecting human-object interactions via functional generalization. In *Proceedings of the AAAI Conference on Artificial Intelligence*, pages 10460–10469, 2020. 6
- [3] Yichao Cao, Qingfei Tang, Xiu Su, Song Chen, Shan You, Xiaobo Lu, and Chang Xu. Detecting any human-object interaction relationship: Universal hoi detector with spatial prompt learning on foundation models. Advances in Neural Information Processing Systems, 36, 2024. 1, 2, 3, 6, 7, 14
- [4] Nicolas Carion, Francisco Massa, Gabriel Synnaeve, Nicolas Usunier, Alexander Kirillov, and Sergey Zagoruyko. End-to-end object detection with transformers. In *European conference on computer vision*, pages 213–229. Springer, 2020. 3, 5, 6, 7, 12
- [5] Yu-Wei Chao, Yunfan Liu, Xieyang Liu, Huayi Zeng, and Jia Deng. Learning to detect human-object interactions. In 2018 ieee winter conference on applications of computer vision (wacv), pages 381–389. IEEE, 2018. 6, 14
- [6] Junwen Chen and Keiji Yanai. Qahoi: query-based anchors for human-object interaction detection. arXiv preprint arXiv:2112.08647, 2021. 2
- [7] Yu Cheng, Yihao Ai, Bo Wang, Xinchao Wang, and Robby T Tan. Bottom-up 2d pose estimation via dual anatomical centers for small-scale persons. *Pattern Recognition*, 139: 109403, 2023. 1
- [8] Alexey Dosovitskiy, Lucas Beyer, Alexander Kolesnikov, Dirk Weissenborn, Xiaohua Zhai, Thomas Unterthiner, Mostafa Dehghani, Matthias Minderer, Georg Heigold, Sylvain Gelly, Jakob Uszkoreit, and Neil Houlsby. An image is worth 16x16 words: Transformers for image recognition at scale. In *International Conference on Learning Representa*tions, 2021. 6
- [9] Abhimanyu Dubey, Abhinav Jauhri, Abhinav Pandey, Abhishek Kadian, Ahmad Al-Dahle, Aiesha Letman, Akhil Mathur, Alan Schelten, Amy Yang, Angela Fan, et al. The llama 3 herd of models. arXiv preprint arXiv:2407.21783, 2024. 3, 14
- [10] Peng Gao, Shijie Geng, Renrui Zhang, Teli Ma, Rongyao Fang, Yongfeng Zhang, Hongsheng Li, and Yu Qiao. Clip-adapter: Better vision-language models with feature adapters. *International Journal of Computer Vision*, 132(2): 581–595, 2024. 3
- [11] Georgia Gkioxari, Ross Girshick, Piotr Dollár, and Kaiming He. Detecting and recognizing human-object interactions. In *Proceedings of the IEEE conference on computer vision and pattern recognition*, pages 8359–8367, 2018. 2
- [12] Xiuye Gu, Tsung-Yi Lin, Weicheng Kuo, and Yin Cui. Open-vocabulary object detection via vision and language

- knowledge distillation. arXiv preprint arXiv:2104.13921, 2021. 1
- [13] Kaiming He, Xiangyu Zhang, Shaoqing Ren, and Jian Sun. Deep residual learning for image recognition. In *Proceedings of the IEEE conference on computer vision and pattern recognition*, pages 770–778, 2016. 6
- [14] Zhi Hou, Xiaojiang Peng, Yu Qiao, and Dacheng Tao. Visual compositional learning for human-object interaction detection. In Computer Vision–ECCV 2020: 16th European Conference, Glasgow, UK, August 23–28, 2020, Proceedings, Part XV 16, pages 584–600. Springer, 2020. 1, 2, 3, 6, 17, 19
- [15] Zhi Hou, Baosheng Yu, Yu Qiao, Xiaojiang Peng, and Dacheng Tao. Affordance transfer learning for human-object interaction detection. In *Proceedings of the IEEE/CVF Con*ference on Computer Vision and Pattern Recognition, pages 495–504, 2021. 3, 14, 19
- [16] Zhi Hou, Baosheng Yu, Yu Qiao, Xiaojiang Peng, and Dacheng Tao. Detecting human-object interaction via fabricated compositional learning. In *Proceedings of the IEEE/CVF Conference on Computer Vision and Pattern Recognition*, pages 14646–14655, 2021. 1, 2, 3, 14, 17
- [17] Edward J Hu, Yelong Shen, Phillip Wallis, Zeyuan Allen-Zhu, Yuanzhi Li, Shean Wang, Lu Wang, and Weizhu Chen. Lora: Low-rank adaptation of large language models. *arXiv* preprint arXiv:2106.09685, 2021. 3
- [18] Menglin Jia, Luming Tang, Bor-Chun Chen, Claire Cardie, Serge Belongie, Bharath Hariharan, and Ser-Nam Lim. Visual prompt tuning. In *European Conference on Computer Vision*, pages 709–727. Springer, 2022. 2, 3
- [19] Muhammad Uzair Khattak, Hanoona Rasheed, Muhammad Maaz, Salman Khan, and Fahad Shahbaz Khan. Maple: Multi-modal prompt learning. In *Proceedings of the IEEE/CVF Conference on Computer Vision and Pattern Recognition*, pages 19113–19122, 2023. 2, 3
- [20] Sanghyun Kim, Deunsol Jung, and Minsu Cho. Relational context learning for human-object interaction detection. In Proceedings of the IEEE/CVF Conference on Computer Vision and Pattern Recognition, pages 2925–2934, 2023. 2
- [21] Yu Kong and Yun Fu. Human action recognition and prediction: A survey. *International Journal of Computer Vision*, 130(5):1366–1401, 2022.
- [22] Qinqian Lei, Bo Wang, and Robby T. Tan. Ez-hoi: Vlm adaptation via guided prompt learning for zero-shot hoi detection. In *The Thirty-eighth Annual Conference on Neural Information Processing Systems*, 2024. 1, 2, 3, 6, 7, 14
- [23] Qinqian Lei, Bo Wang, and Robby T Tan. Few-shot learning from augmented label-uncertain queries in bongard-hoi. In *Proceedings of the AAAI Conference on Artificial Intelligence*, pages 2974–2982, 2024.
- [24] Ting Lei, Fabian Caba, Qingchao Chen, Hailin Jin, Yuxin Peng, and Yang Liu. Efficient adaptive human-object interaction detection with concept-guided memory. In *Proceedings* of the IEEE/CVF International Conference on Computer Vision, pages 6480–6490, 2023. 1, 2, 3, 6, 7, 12, 14, 19
- [25] Ting Lei, Shaofeng Yin, and Yang Liu. Exploring the potential of large foundation models for open-vocabulary hoi

- detection. In *Proceedings of the IEEE/CVF Conference on Computer Vision and Pattern Recognition (CVPR)*, pages 16657–16667, 2024. 18
- [26] Ting Lei, Shaofeng Yin, Yuxin Peng, and Yang Liu. Exploring conditional multi-modal prompts for zero-shot hoi detection. In *European Conference on Computer Vision*, pages 1–19. Springer, 2024. 1, 2, 3, 6, 7, 14
- [27] Junnan Li, Dongxu Li, Caiming Xiong, and Steven Hoi. Blip: Bootstrapping language-image pre-training for unified vision-language understanding and generation. In *International Conference on Machine Learning*, pages 12888–12900. PMLR, 2022. 3
- [28] Junnan Li, Dongxu Li, Silvio Savarese, and Steven Hoi. Blip-2: Bootstrapping language-image pre-training with frozen image encoders and large language models. arXiv preprint arXiv:2301.12597, 2023. 3
- [29] Liulei Li, Jianan Wei, Wenguan Wang, and Yi Yang. Neurallogic human-object interaction detection. Advances in Neural Information Processing Systems, 36, 2024. 2, 6, 7, 14
- [30] Yue Liao, Aixi Zhang, Miao Lu, Yongliang Wang, Xiaobo Li, and Si Liu. Gen-vlkt: Simplify association and enhance interaction understanding for hoi detection. In *Proceedings of the IEEE/CVF Conference on Computer Vision and Pattern Recognition (CVPR)*, pages 20123–20132, 2022. 1, 2, 3, 6, 7, 14
- [31] Tsung-Yi Lin, Michael Maire, Serge Belongie, James Hays, Pietro Perona, Deva Ramanan, Piotr Dollár, and C Lawrence Zitnick. Microsoft coco: Common objects in context. In Computer Vision–ECCV 2014: 13th European Conference, Zurich, Switzerland, September 6-12, 2014, Proceedings, Part V 13, pages 740–755. Springer, 2014. 14
- [32] Tsung-Yi Lin, Priya Goyal, Ross Girshick, Kaiming He, and Piotr Dollár. Focal loss for dense object detection. In *Proceedings of the IEEE international conference on computer vision*, pages 2980–2988, 2017. 5
- [33] Haotian Liu, Chunyuan Li, Yuheng Li, and Yong Jae Lee. Improved baselines with visual instruction tuning. *arXiv* preprint arXiv:2310.03744, 2023. 3
- [34] Haotian Liu, Chunyuan Li, Qingyang Wu, and Yong Jae Lee. Visual instruction tuning. *Advances in neural information processing systems*, 36:34892–34916, 2023. 3, 14
- [35] Ilya Loshchilov and Frank Hutter. Decoupled weight decay regularization. arXiv preprint arXiv:1711.05101, 2017. 14
- [36] Jinguo Luo, Weihong Ren, Weibo Jiang, Xi'ai Chen, Qiang Wang, Zhi Han, and Honghai Liu. Discovering syntactic interaction clues for human-object interaction detection. In *Proceedings of the IEEE/CVF Conference on Computer Vision and Pattern Recognition*, pages 28212–28222, 2024. 2
- [37] Yunyao Mao, Jiajun Deng, Wengang Zhou, Li Li, Yao Fang, and Houqiang Li. Clip4hoi: Towards adapting clip for practical zero-shot hoi detection. Advances in Neural Information Processing Systems, 36, 2024. 1, 2, 3, 6, 7, 14
- [38] Matthias Minderer, Alexey Gritsenko, Austin Stone, Maxim Neumann, Dirk Weissenborn, Alexey Dosovitskiy, Aravindh Mahendran, Anurag Arnab, Mostafa Dehghani, Zhuoran Shen, et al. Simple open-vocabulary object detection. In *European Conference on Computer Vision*, pages 728–755. Springer, 2022. 1

- [39] Shan Ning, Longtian Qiu, Yongfei Liu, and Xuming He. Hoiclip: Efficient knowledge transfer for hoi detection with vision-language models. In *Proceedings of the IEEE/CVF* Conference on Computer Vision and Pattern Recognition, pages 23507–23517, 2023. 1, 2, 3, 6, 7, 8, 14, 17
- [40] Jeeseung Park, Jin-Woo Park, and Jong-Seok Lee. Viplo: Vision transformer based pose-conditioned self-loop graph for human-object interaction detection. In *Proceedings of* the IEEE/CVF Conference on Computer Vision and Pattern Recognition, pages 17152–17162, 2023. 2
- [41] Xian Qu, Changxing Ding, Xingao Li, Xubin Zhong, and Dacheng Tao. Distillation using oracle queries for transformer-based human-object interaction detection. In *Proceedings of the IEEE/CVF Conference on Computer Vision and Pattern Recognition*, pages 19558–19567, 2022. 2
- [42] Alec Radford, Jong Wook Kim, Chris Hallacy, Aditya Ramesh, Gabriel Goh, Sandhini Agarwal, Girish Sastry, Amanda Askell, Pamela Mishkin, Jack Clark, et al. Learning transferable visual models from natural language supervision. In *International conference on machine learning*, pages 8748–8763. PMLR, 2021. 2, 3, 4
- [43] Pau Rodríguez, Jordi Gonzalez, Guillem Cucurull, Josep M Gonfaus, and Xavier Roca. Regularizing cnns with locally constrained decorrelations. arXiv preprint arXiv:1611.01967, 2016. 4
- [44] Manli Shu, Weili Nie, De-An Huang, Zhiding Yu, Tom Goldstein, Anima Anandkumar, and Chaowei Xiao. Test-time prompt tuning for zero-shot generalization in vision-language models. *Advances in Neural Information Processing Systems*, 35:14274–14289, 2022. 2, 3
- [45] Mohammed Suhail, Abhay Mittal, Behjat Siddiquie, Chris Broaddus, Jayan Eledath, Gerard Medioni, and Leonid Sigal. Energy-based learning for scene graph generation. In *Proceedings of the IEEE/CVF conference on computer vision and pattern recognition*, pages 13936–13945, 2021. 1
- [46] Yi-Lin Sung, Jaemin Cho, and Mohit Bansal. Vl-adapter: Parameter-efficient transfer learning for vision-and-language tasks. In Proceedings of the IEEE/CVF conference on computer vision and pattern recognition, pages 5227–5237, 2022. 3
- [47] Masato Tamura, Hiroki Ohashi, and Tomoaki Yoshinaga. Qpic: Query-based pairwise human-object interaction detection with image-wide contextual information. In *Proceedings of the IEEE/CVF Conference on Computer Vision and Pattern Recognition*, pages 10410–10419, 2021. 2
- [48] Guangzhi Wang, Yangyang Guo, Ziwei Xu, and Mohan Kankanhalli. Bilateral adaptation for human-object interaction detection with occlusion-robustness. In *Proceedings of* the IEEE/CVF Conference on Computer Vision and Pattern Recognition, pages 27970–27980, 2024. 2
- [49] Eastman ZY Wu, Yali Li, Yuan Wang, and Shengjin Wang. Exploring pose-aware human-object interaction via hybrid learning. In Proceedings of the IEEE/CVF Conference on Computer Vision and Pattern Recognition, pages 17815– 17825, 2024. 2
- [50] Mingrui Wu, Jiaxin Gu, Yunhang Shen, Mingbao Lin, Chao Chen, and Xiaoshuai Sun. End-to-end zero-shot hoi detec-

- tion via vision and language knowledge distillation. In *Proceedings of the AAAI Conference on Artificial Intelligence*, pages 2839–2846, 2023. 3, 14, 17
- [51] Chi Xie, Fangao Zeng, Yue Hu, Shuang Liang, and Yichen Wei. Category query learning for human-object interaction classification. In *Proceedings of the IEEE/CVF Conference* on Computer Vision and Pattern Recognition, pages 15275– 15284, 2023. 2
- [52] Xianghui Xie, Bharat Lal Bhatnagar, and Gerard Pons-Moll. Chore: Contact, human and object reconstruction from a single rgb image. In *European Conference on Computer Vision*, pages 125–145. Springer, 2022. 1
- [53] Jie Yang, Bingliang Li, Ailing Zeng, Lei Zhang, and Ruimao Zhang. Open-world human-object interaction detection via multi-modal prompts. In *Proceedings of the IEEE/CVF Con*ference on Computer Vision and Pattern Recognition, pages 16954–16964, 2024. 18
- [54] Lingxiao Yang, Ru-Yuan Zhang, Yanchen Wang, and Xiao-hua Xie. Mma: Multi-modal adapter for vision-language models. In *Proceedings of the IEEE/CVF Conference on Computer Vision and Pattern Recognition*, pages 23826–23837, 2024. 3
- [55] Hangjie Yuan, Jianwen Jiang, Samuel Albanie, Tao Feng, Ziyuan Huang, Dong Ni, and Mingqian Tang. Rlip: Relational language-image pre-training for human-object interaction detection. Advances in Neural Information Processing Systems, 35:37416–37431, 2022. 2
- [56] Yuhang Zang, Wei Li, Kaiyang Zhou, Chen Huang, and Chen Change Loy. Unified vision and language prompt learning. arXiv preprint arXiv:2210.07225, 2022. 2, 3
- [57] Alireza Zareian, Kevin Dela Rosa, Derek Hao Hu, and Shih-Fu Chang. Open-vocabulary object detection using captions. In Proceedings of the IEEE/CVF Conference on Computer Vision and Pattern Recognition, pages 14393–14402, 2021.
- [58] Frederic Z Zhang, Dylan Campbell, and Stephen Gould. Spatially conditioned graphs for detecting human-object interactions. In *Proceedings of the IEEE/CVF International Conference on Computer Vision*, pages 13319–13327, 2021. 2, 3, 6
- [59] Frederic Z Zhang, Dylan Campbell, and Stephen Gould. Efficient two-stage detection of human-object interactions with a novel unary-pairwise transformer. In *Proceedings of* the IEEE/CVF Conference on Computer Vision and Pattern Recognition, pages 20104–20112, 2022. 2, 3, 6
- [60] Frederic Z Zhang, Yuhui Yuan, Dylan Campbell, Zhuoyao Zhong, and Stephen Gould. Exploring predicate visual context in detecting of human-object interactions. In *Proceedings of the IEEE/CVF International Conference on Computer Vision*, pages 10411–10421, 2023. 2
- [61] Jason Y Zhang, Sam Pepose, Hanbyul Joo, Deva Ramanan, Jitendra Malik, and Angjoo Kanazawa. Perceiving 3d human-object spatial arrangements from a single image in the wild. In Computer Vision–ECCV 2020: 16th European Conference, Glasgow, UK, August 23–28, 2020, Proceedings, Part XII 16, pages 34–51. Springer, 2020. 1
- [62] Renrui Zhang, Rongyao Fang, Wei Zhang, Peng Gao, Kunchang Li, Jifeng Dai, Yu Qiao, and Hongsheng Li.

- Tip-adapter: Training-free clip-adapter for better vision-language modeling. *arXiv preprint arXiv:2111.03930*, 2021.
- [63] Xin Zhang and Robby T. Tan. Mamba as a bridge: Where vision foundation models meet vision language models for domain-generalized semantic segmentation. In *Proceedings* of the IEEE/CVF Conference on Computer Vision and Pattern Recognition (CVPR), pages 14527–14537, 2025. 1
- [64] Kaiyang Zhou, Jingkang Yang, Chen Change Loy, and Ziwei Liu. Conditional prompt learning for vision-language models. In Proceedings of the IEEE/CVF conference on computer vision and pattern recognition, pages 16816–16825, 2022. 3
- [65] Kaiyang Zhou, Jingkang Yang, Chen Change Loy, and Ziwei Liu. Learning to prompt for vision-language models. *International Journal of Computer Vision*, 130(9):2337–2348, 2022. 2, 3
- [66] Cheng Zou, Bohan Wang, Yue Hu, Junqi Liu, Qian Wu, Yu Zhao, Boxun Li, Chenguang Zhang, Chi Zhang, Yichen Wei, et al. End-to-end human object interaction detection with hoi transformer. In *Proceedings of the IEEE/CVF conference on computer vision and pattern recognition*, pages 11825–11834, 2021. 2, 6

Supplementary Material

A. Vision Branch

The detailed vision branch is illustrated in Fig. 7. We first leverage a pre-trained DETR [4] model for object detection, identifying all detected humans and objects h_i, o_j , where $i \in \{1, 2, \cdots, n_h\}, j \in \{1, 2, \cdots, n_o\}$. Here, n_h and n_o represent the total number of detected humans and objects, respectively. For each detection, we extract human and object features from the DETR decoder, denoted as f_{h_i} and f_{o_j} . We then generate all possible human-object feature pairs, represented as (f_{h_i}, f_{o_j}) . The human-object tokens are computed as :

$$T_{\text{ho}_{ij}} = \frac{f_{h_i} + f_{o_j}}{2} + f_{\text{ho}_{ij}}^{\text{spatial}}, \tag{11}$$

where $f_{\mathrm{ho}_{ij}}^{\mathrm{spatial}}$ is derived from human-object bounding boxes, incorporating the center coordinates, width, height of each box, pairwise intersection-over-union (IoU), and relative area, which are then processed through an MLP together to obtain $f_{\mathrm{ho}_{ij}}^{\mathrm{spatial}}$. Thus, $T_{\mathrm{ho}_{ij}}$ integrates both appearance and spatial cues to enhance interaction representation for each human-object feature pair (f_{h_i}, f_{o_j}) . The complete set of human-object tokens is denoted as T_{ho} , where $T_{\mathrm{ho}} = \{T_{\mathrm{ho}_{ij}} \mid 1 \leq i \leq n_h, 1 \leq j \leq n_o\}$.

To further incorporate interaction prior knowledge, we leverage an LLM to generate descriptions of human body configurations, object attributes, and their spatial relationships with humans. These descriptions are then encoded by the VLM text encoder to obtain prior knowledge features $f_{\rm ho}^{\rm pr}$. An example of the generated descriptions used to capture human-object interaction prior knowledge is provided at the end of this section.

To integrate prior-knowledge features $f_{
m ho}^{
m pr}$ with human-object tokens, we design a cross-attention module: First, down and up projection layers are used to reduce computational cost. Next, human-object tokens serve as the query, while prior-knowledge features $f_{
m ho}^{
m pr}$ act as the key and value in the cross-attention mechanism. Finally, a residual connection adds the input human-object tokens back to the cross-attention output, refining interaction representation while preserving the original information.

The output human-object tokens are concatenated with input image patches and fed into the VLM visual encoder, guiding it to focus on human-object interactions and improving action distinction. To enhance adaptability, we insert the adapter [24] between each layer of the visual encoder. The output includes adapted human-object tokens \hat{T}_{ho} and an image feature map $f_{img}^{glb} \in \mathcal{R}^{H \times W \times d}$. The final HOI image feature, denoted as $f_{img} \in \mathcal{R}^{d \times 1}$ and used by the weight adaptation, is defined as follows:

$$f_{\text{img}} = \frac{1}{H * W} \sum_{i=1}^{H} \sum_{j=1}^{W} f_{\text{img}}^{\text{glb}}(i, j, :).$$
 (12)

We denote the detected bounding boxes for the human, object, and their union regions as b_h , b_o , and b_u , respectively. To extract features focused on specific human-object interaction regions within the image, we first apply RoI pooling to obtain region-specific features of dimension $p \times p \times d$, where p is set to 7. We then apply spatial average pooling to each region-specific feature to obtain $f_{\rm img}^h, f_{\rm img}^o, f_{\rm img}^u$.

The image fusion module is designed to combine the human and object features $f_{\rm img}^h$ and $f_{\rm img}^o$, respectively. The image fusion process takes the concat $(f_{\rm img}^h, f_{\rm img}^o)$ as input and outputs $f_{\rm img}^{\rm ho}$. Here, concat denotes concatenation of two features along the first dimension. To reduce computational cost, the image fusion module incorporates down and up projection layers. The concatenated input features then pass through a self-attention module, integrating action and object visual features. Finally, a residual connection adds the input back to the output, refining the fusion while preserving input information.

According to Eq.(8) of the main paper, we compute the action prediction s_a . For convenience, we reproduce the equation below:

$$s_a = \gamma_1 * (\sin(f_{\text{img}}^u, \mathbf{\hat{F}}) + \sin(\hat{T}_{\text{ho}}, \mathbf{\hat{F}})) * l_u^R +$$

$$\gamma_2 * \sin(f_{\text{img}}^{\text{ho}}, \mathbf{\hat{F}}^{\text{ao}}) * l_{ao}^R.$$
(13)

Here is an example prompt used with an LLM to generate prior knowledge for the human-object pair \langle human, car \rangle .

Provide a detailed description of the physical relationship between a given human-object pair, focusing on various possible configurations and spatial relationships without assuming or naming specific interactions. For the pair (human, car), describing the following perspectives:

- 1. **Human Body Description: ** Describe the positioning and orientation of key body parts (e.g., hands, feet, arms, legs, torso, head) in relation to the object. Highlight the possible roles of specific body parts (e.g., hands gripping, feet pressing, or knees bending) without specifying actions.
- 2. **Object Description:** Provide a clear and concise description of the object, focusing on its relative size, shape, and structure compared to the human in the image. Include details about key components (e.g., wheels, deck from skateboard) and their spatial relationship to the human body in various scenarios. Highlight how the object might be positioned (e.g., sliced, tilted, vertical) and how its components could interact with specific body parts of the human.

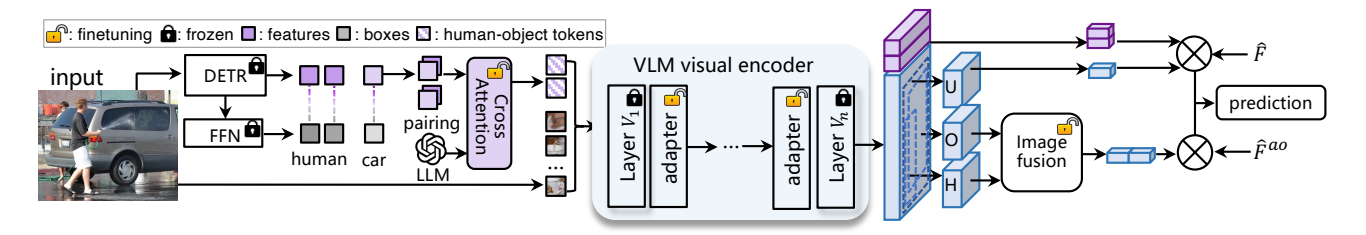


Figure 7. Overview of our vision branch.

The goal is to provide a comprehensive pool of descriptive information for the human, object, and their possible configurations in various scenarios. Avoid limiting the scope by naming specific interactions or actions. Focus instead on a rich and versatile set of physical relationships. Focus on critical details, avoiding redundant or non-essential information to ensure clarity and precision.

The following is the prior knowledge generated by the LLM for the human–car pair:

1. Human Body Description: (a) Positioning and Orientation: - Head: The human's head can be oriented in various directions relative to the car, such as facing towards the car, away from it, or to the sides. The head's angle might vary, possibly tilted up or down, depending on the human's position relative to the car's height, such as looking over the roof or under the chassis. - Torso: The torso may be upright, leaning forward, or angled sideways. Its position could vary significantly depending on proximity to the car, such as standing next to it, bending over the hood, or leaning against the side. - Arms and Hands: The arms might be extended towards the car or resting at the sides. Hands can be positioned near various parts of the car, such as the door handles, mirrors, or hood, suggesting a potential for contact or proximity. - Legs and Feet: Legs could be positioned straight, bent, or spread apart, depending on the stance relative to the car. Feet might be placed firmly on the ground, perhaps transitioning from one side of the car to the other, or positioned close to the wheels or undercarriage. (b) Roles of Specific Body Parts: - Hands: The hands might appear poised to make contact with the car's surface, potentially hovering over or near tactile features like handles or mirrors. - Feet: The feet might be aligned parallel to the car or angled towards it, suggesting readiness for movement or balance. - Knees: Knees might be straight or slightly bent, indicating a stance that accommodates reaching or observing different parts of the car.

2. Object Description: (a) Size, Shape, and Structure: General Structure: The car is a relatively large object compared to a human, with a defined structure typically including a body, wheels, and windows. It is generally elongated with a front (hood), middle (cabin), and rear (trunk). - Key Components: - Wheels: Typically four, located at the corners of the car, often near the ground and could be aligned

with the human's feet or legs. - Body Panels: Including doors, hood, trunk, and roof, which vary in height and shape, potentially aligning with the human's torso or head. - Windows and Mirrors: Positioned at varying heights, likely matching the human's eye level or above, affecting the head's orientation.

B. Language Branch

We leverage the LLM to generate descriptions for both HOI and action classes in the language branch.

HOI Description Generation The descriptions for all given HOI classes are utilized to obtain the VLM text features **F** through the VLM text encoder, as discussed in Section 3.1 of the main paper. For a detailed illustration, consider the HOI class "hosing a car" as an example. The description generated for this HOI class is as follows:

"Hosing a car" description: The photo shows a person using a hose to clean or wash a car. Common elements include water, soap, cleaning tools, and the person's attention to various parts of the car's exterior.

Action Description Generation Additionally, we introduce action descriptions for all given action classes to obtain action regularization, as discussed in Section 3.2 of the main paper.

Here is an example prompt provided to the LLM to generate a description for the action "hose".

Please describe the visual features for action: hose. The objects can be "car, dog, potted plant, elephant". Please summarize the common visual features for the action, shared by the objects. Use LESS than 250 characters for description."

The following is the action description generated by the LLM for "hose":

The visual features for the action "a person is hosing the object" include: 1. Person holding a hose or water spray nozzle. 2. Object being hosed (e.g. car, dog, potted plant, elephant) in close proximity to the person. 3. Water spray or stream visible, potentially creating a mist or splash. 4. Person's arm or hand in motion, indicating the action of spraying water. 5. Background context suggesting an outdoor or yard setting.

C. Experiment Results

C.1. Implementation Details

In weight adaptation, image and text fusion and humanobject tokens design, all down projection layers reduce feature dimension from 512 to 64, while all up projection layers expands it back from 64 to 512. The head number of self attention and cross attention modules is 2. The temperature of KL divergence used in our method is 0.1. We use AdamW [35] as the optimizer and the initial learning rate is 1e-3. For all experiments, our batch size is set as 64 on 4 A5000 GPUs. Training takes 7 hours on 4 A5000 GPUs (22.5 GB VRAM each) with only 4.0M trainable parameters. Inference time is 82 ms per image.

We use three types of descriptions generated by foundation models: (1) HOI class descriptions from EZ-HOI [22], generated using LLaVA [34]. These descriptions are encoded by a VLM text encoder to produce **F**, as described in Section 3.1 (VLM Feature Decomposition and Adaptation) of the main paper. An example is also included in the HOI Description Generation subsection of the language branch (Appendix B); (2) action descriptions for LLM-derived action regularization, generated using the LLaMA-3-8B model [9], and used in the language branch (Appendix B); and (3) Prior knowledge descriptions for human-object pairs, also generated by LLaMA-3-8B, and used in the vision branch (Appendix A).

Datasets We evaluate our method on the HICO-DET dataset [5], a widely-used benchmark in human-object interaction detection. HICO-DET contains 47,776 images in total, consisting of 38,118 training images and 9,658 test images. The dataset includes 600 HOI classes combined from 117 action categories and 80 object categories. We also provided the evaluation on the V-COCO [31], a subset of COCO, comprises 10,396 images, with 5,400 trainval images and 4,946 test images, and includes 24 action classes and 80 object classes. Note that V-COCO only contains evaluation under fully-supervised setting, but our focus is on the zero-shot HOI detection.

C.2. Quantitative Results

Fully Supervised Setting on HICO-DET We evaluate our method against HOI approaches with zero-shot HOI detection ability in the fully supervised settings, excluding methods that do not support unseen-action HOI detection. Table 8 demonstrates that our method sets a new state-of-the-art performance on the HICO-DET dataset in the fully supervised setting. Using the ViT-B backbone, the same as those used in existing methods [3, 15, 16, 26, 29, 30, 37, 39, 50], our method achieves a 35.41 mAP, surpassing all state-of-the-art two-stage HOI detection methods. Switching to a ViT-L backbone further enhances performance, reaching 39.05 mAP. Although primarily designed to focus on

		HICO-D	ET
Method	Full	Rare	Nonrare
One-stage Methods			
GEN-VLKT (CVPR'22) [30]	33.75	29.25	35.10
EoID (AAAI'23) [50]	31.11	26.49	32.49
HOICLIP (CVPR'23) [39]	34.69	31.12	35.74
LogicHOI (NeurIPS'23) [29]	35.47	32.03	<u>36.22</u>
UniHOI (NeurIPS'23) [3]	35.92	34.39	36.26
Two-stage Methods			
FCL (CVPR'21) [16]	29.12	23.67	30.75
ATL (CVPR'21) [15]	23.81	17.43	25.72
ADA-CM [24] (ICCV'23)	33.80	31.72	34.42
CLIP4HOI (NeurIPS'23) [37]	<u>35.33</u>	<u>33.95</u>	35.75
CMMP (ECCV'24) [26]	33.24	32.26	33.53
Ours (HOLa)	35.41	34.35	<u>35.73</u>
ADA-CM _l (ICCV'23)	38.40	37.52	38.66
CMMP _l (ECCV'24)	38.14	<u>37.75</u>	38.25
EZ-HOI _l (NeurIPS'24)	38.61	37.70	38.89
Ours _l (HOLa)	39.05	38.66	39.17

Table 8. Quantitative comparison of HOI detection with state-of-the-art methods in the fully-supervised setting on HICO-DET. *Ours*₁ denotes our scaled-up version utilizing the ViT-L/14 backbone.

zero-shot HOI detection and improve generalization to unseen classes, our method also shows competitive results in the fully supervised setting, underscoring its effectiveness across diverse evaluation scenarios.

Fully Supervised Setting on V-COCO Our method also demonstrates competitive performance on the V-COCO dataset, achieving a 66.0 $AP_{role}^{S_2}$, achieving an improvement of 2.0 mAP over the current state-of-the-art method, CMMP [26]. Our $AP_{role}^{S_1}=60.3$.

C.3. Ablation Study

Rank Selection for B and W We conduct an ablation study on the rank m of the basis features and weights, as shown in Table 9. This study specifically explores the impact of the selected rank m on the performance, focusing solely on the feature decomposition module. Consequently, other components, such as the action prior and the action-object branch, were excluded from this analysis.

We initialize the weights and basis features using Principal Component Analysis (PCA). Specifically, we achieve reconstruction percentages of 0.80, 0.90, 0.95, and 0.98 for the original VLM text features, **F**. These percentages correspond to ranks of 17, 42, 71, and 119, respectively, in the obtained weights and basis features.

The evaluation results show that a rank 17 yields the highest unseen mAP (26.32), due to its compact representation that emphasizes class-shared features, enhancing gen-

reconstruction	rank	mAP		
score	Talik	Unseen	Seen	Full
0.80	17	26.32	32.69	31.80
0.90	42	25.71	33.01	31.98
0.95	71	25.47	33.59	32.46
0.98	119	25.17	32.82	31.75

Table 9. Ablation study for the rank of basis features \mathbf{B} and weights \mathbf{W} in the unseen-verb zero-shot setting.

т	т		mAP	
$L_{ m ort}$	$L_{\rm sparse}$	Unseen	Seen	Full
$\overline{}$	✓	26.81	34.70	33.60
\checkmark	×	27.47	34.45	33.48
\checkmark	\checkmark	27.91	35.09	34.09

Table 10. Ablation study for VLM feature decomposition constraints $L_{\rm ort}$ and $L_{\rm sparse}$ in the unseen-verb zero-shot setting.

eralization to unseen classes. However, this compactness leads to a drop in seen class performance, due to the loss of some detailed information from **F**. Conversely, increasing the rank to 119 captures more class-specific details in the reconstructed features but diminishes the shared information across classes, leading to poorer unseen class performance. Consequently, we select the rank of 71 to optimally balance performance between seen and unseen classes.

VLM Feature Decomposition Constraints We conducted an ablation study on the constraints for VLM feature decomposition as shown in Table 10. The first row removes the orthogonal constraint $L_{\rm ort}$ on the basis features, leading to 1.10 mAP drop among unseen classes compared to the third row, indicating that the orthogonal constraint helps the basis features capture class-shared information more effectively, enhancing generalization to unseen classes. Additionally, removing the sparsity constraint $L_{\rm sparse}$ (second row) lowers both seen and unseen performance, indicating that sparsity reduces redundancy in the factorization, leading to a more compact representation.

Semantic Loss We also design the semantic loss $L_{\rm sem}$ to preserve the distribution of pairwise cosine similarity among VLM text feature of each class. The pairwise cosine similarity demonstrates the relationship between HOI classes indicated by VLM, which, trained on millions of data, generalizes these relationships to unseen classes. Unlike the original VLM features, which primarily emphasize object information and cluster different actions with the same object together, our method explicitly enhances action distinctions. To achieve this, we compute similarity only among HOI classes involving the same object, as shown in Eq.(14), with the mask M excluding interactions with different objects.

т	mAP				
$L_{\rm sem}$	Unseen	Seen	Full		
×	27.19	34.68	33.63		
\checkmark	27.91	35.09	34.09		

Table 11. Ablation study for semantic loss in the unseen-verb zeroshot setting.

LLM-generated	mAP			
Prior Knowledge	Unseen	Seen	Full	
×	27.90	34.58	33.65	
\checkmark	27.91	35.09	34.09	

Table 12. Ablation study for LLM description in human-object token design of the vision branch. "None" means no interaction prior knowledge generated from LLM.

$$L_{\text{sem}} = D_{\text{KL}} \left[\frac{\sin(\hat{\mathbf{F}}, \hat{\mathbf{F}})}{\tau} * M \parallel \frac{\sin(\mathbf{F}, \mathbf{F})}{\tau} * M \right] + D_{\text{KL}} \left[\frac{\sin(\hat{\mathbf{F}}^{ao}, \hat{\mathbf{F}}^{ao})}{\tau} * M \parallel \frac{\sin(\mathbf{F}, \mathbf{F})}{\tau} * M \right],$$
(14)

where we apply a temperature coefficient τ in the KL divergence, setting $\tau=0.1$ to emphasize action relationships that are underestimated in the original VLM features. As shown in Table 11, without $L_{\rm sem}$, the overall performance in the unseen-verb setting decreases from 32.66 to 32.41 mAP, with a 0.48 mAP drop among unseen classes.

Human-Object Tokens Table 12 presents the ablation study on interaction prior knowledge generated by the LLM for human-object tokens $f_{\rm ho}$. In the first row, we remove this prior knowledge and replace cross-attention with self-attention process for $f_{\rm ho}$. The results indicate that interaction prior knowledge primarily improves seen-class performance. This is because the interaction prior knowledge provides all possible human body configurations, object attributes and their spatial relationships. During training, the model is guided by training data to select knowledge mainly for seen HOI classes. Consequently, this interaction prior knowledge does not obviously enhance unseen HOI performance.

Table 13 shows the ablation study on the components of human-object tokens $f_{\text{ho}_{ij}}$. As defined in Eq.(11), $f_{\text{ho}_{ij}}$ consists of two components: human and object appearance features $\frac{f_{h_i}+f_{o_j}}{2}$ from DETR and the spatial features $f_{\text{ho}_{ij}}^{\text{spatial}}$ from detected human and object bounding boxes. We found that we need to combine all components in human-object tokens for the best performance among both seen and unseen classes according to the results shown in Table 13.

Image Fusion Table 14 presents the ablation study for the

f	mAP			
$f_{\mathrm{ho}_{ij}}$	Unseen	Seen	Full	
$\frac{f_{h_i}+f_{o_j}}{2}$	27.37	34.42	33.43	
$f_{\mathrm{ho}_{ii}}^{\mathrm{spatial}}$	27.59	34.63	33.64	
$f_{ ext{ho}_{ij}}^{ ext{spatial}} = rac{f_{ ext{ho}_{ij}}}{2} + f_{ ext{ho}_{ij}}^{ ext{spatial}}$	27.91	35.09	34.09	

Table 13. Ablation study for human-object token design of the vision branch. "None" means no interaction prior knowledge generated from LLM.

Imaga Eusian	mAP			
Image Fusion	Unseen	Seen	Full	
×	26.46	34.19	33.10	
\checkmark	27.91	35.09	34.09	

Table 14. Ablation study for image fusion design in the unseenverb zero-shot setting.

image fusion module. Removing this module reduces performance from 34.09 to 33.10 mAP, highlighting its effectiveness. The image fusion module adapts and integrates separate action and object visual features, capturing more fine-grained information than human-object union region features. While $f_{\rm img}^h$, $f_{\rm img}^o$, and $f_{\rm img}^u$ share the same feature dimension, $f_{\rm img}^h$ and $f_{\rm img}^o$ focus on smaller, localized regions—human and object separately, rather than their combined union. This processing better preserves action and object details, ultimately improving performance.

VLM Feature Decomposition and Adaptation Table 15 presents an ablation study on the VLM feature decomposition and adaptation. The first row serves as the baseline, where VLM feature decomposition is not applied, and no LLM-derived regularization are used. This baseline ensures that the ablation study specifically analyzes the impact of VLM feature decomposition. In the second row, we apply the only feature decomposition loss $L_{\rm fd}$ to update both weights and basis features $(\overline{W}, \overline{B})$. This improves unseen mAP by 2.18, indicating that feature decomposition enhances generalization to unseen classes. Applying classification loss L_{cls} only to the basis features ($\overline{\mathbf{W}}$, \mathbf{B}), as in the third row, yields results similar to the second row. In the fourth row, adding classification loss L_{cls} , supervised by ground truths from seen classes together with $L_{\rm fd}$ in the training process, to both weights and basis features results in performance degradation (W, B). This suggests that the updating of basis features from training data compromises essential class-shared information necessary for generalization, while the weights do not adapt effectively to distinguish actions within the HOI setting. The last row shows the best results, where L_{cls} is applied only to the weights, while $L_{\rm fd}$ is used for both weights and basis features (W, $\overline{\bf B}$). This

w B		mAP			
W B	Unseen	Seen	Full		
/	/	23.58	31.55	30.43	
$\overline{\mathbf{W}}$	$\overline{\mathbf{B}}$	25.76	31.35	30.57	
$\overline{\mathbf{W}}$	В	25.84	31.19	30.44	
\mathbf{W}	В	22.95	30.30	29.27	
\mathbf{W}	$\overline{\mathbf{B}}$	25.47	33.59	32.46	

Table 15. Ablation study for weights and basis features optimization in the unseen-verb zero-shot setting. \mathbf{X} denotes applying classification loss $L_{\rm cls}$ and feature decomposition loss $L_{\rm fd}$ in training to update \mathbf{X} . $\overline{\mathbf{X}}$ denotes applying only $L_{\rm fd}$. $\mathbf{X} \in \{\mathbf{W}, \mathbf{B}\}$.

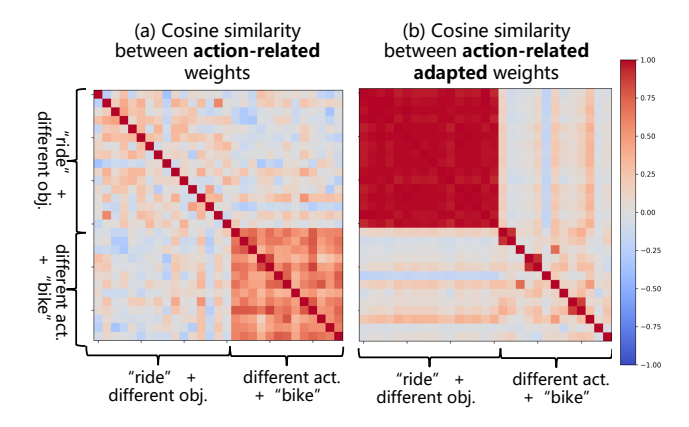


Figure 8. (a) Weight subset similarity visualization related to "ride" and "bike" HOI classes, **before weight adaptation**; (b) Adapted weight subset similarity visualization related to "ride" and "bike" HOI classes, **after weight adaptation**.

configuration achieves balanced performance across seen and unseen classes, improving the seen mAP by 2.04 and the unseen mAP by 1.89 compared to the baseline.

Weights for each training loss term Loss weights including α , β_1 , β_2 , β_3 , β_4 introduced in Section 3.4 of the main paper, are set to keep all loss terms on a comparable scale during early training, ensuring balanced contributions. Table 16 shows an ablation study where we vary one loss weight at a time while keeping the others fixed, where using comparable values for each loss term results in the best overall performance.

Visual Features for Human, Object and Union Regions We use three visual features from the image feature map $f_{\rm img}^{\rm glb}$ for HOI prediction: human $(f_{\rm img}^h)$, object $(f_{\rm img}^o)$, and union $(f_{\rm img}^u)$ features. Ablation results in Table 17 show that using all three yields the best performance.

Weight Adaptation Visualization Here, we visualize and compare the weights W before and after the weight adaptation process, especially focusing on the subset of W applied with the LLM-derived action regularization, as discussed in the main paper Section 3.2. The index set for the subset selection is defined as $\mathcal{I} = \{i \mid b_i \in \mathbf{B}^a\}$, where b_i is

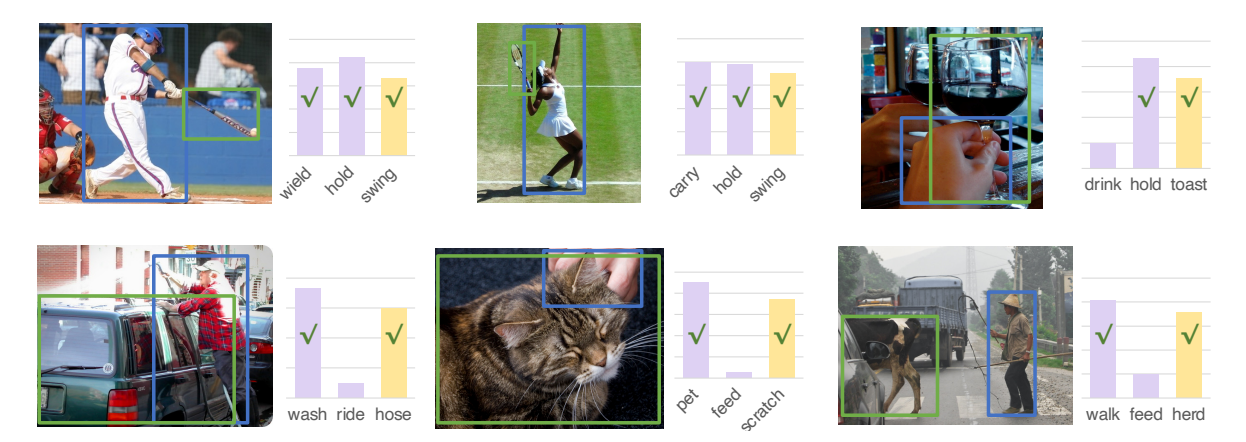


Figure 9. Visualization of HOI predictions in the unseen-verb setting on HICO-DET. The purple bar indicates predictions for seen HOI classes and the yellow bar indicates predictions for unseen HOI classes.

	0	0	Q	0	mAP		
α	ρ_1	β_2	β_3	β_4	Unseen	Seen	Full
320	0.1	0.1	0.001	50	27.50	33.95	33.05
80	0.5	0.1	0.001	50	28.32	34.35	33.50
80	0.1	0.5	0.001	50	28.81	34.64	33.82
80	0.1	0.1	0.005	50	27.12	34.38	33.36
80	0.1	0.1	0.001	250	27.87	33.69	32.88
80	0.1	0.1	0.001	50	27.91	35.09	34.09

Table 16. Ablation study for training loss weights in the unseenverb zero-shot setting. In each row, one loss weight is varied while others remain fixed. The changed value is shown in blue.

		mAP	
	Unseen	Seen	Full
H+U	27.92	33.80	32.98
O+U	27.58	33.95	33.06
H+O	27.36	34.81	33.76
H+O+U	27.91	35.09	34.09

Table 17. Ablation study on visual features in the vision branch under the unseen-verb zero-shot setting. "H", "O", and "U" denote $f_{\rm img}^h$, $f_{\rm img}^o$, and $f_{\rm img}^u$, respectively.

the i-th row of the matrix \mathbf{B} and also belongs to the subset \mathbf{B}^a Before weight adaptation, the subset of \mathbf{W} is obtained by $\{\boldsymbol{w}_i' \mid i \in \mathcal{I}\}$, where \boldsymbol{w}_i' is the i-th column of the matrix \mathbf{W} . After weight adaptation, the subset is denoted as $\mathbf{W}_{\mathrm{ar}} = \{\hat{w}_i' \mid i \in \mathcal{I}\}$, where \hat{w}_i' is the i-th column of the adapted matrix \mathbf{W} .

As shown in Fig. 8 (a), the subset before the weight adaptation contains limited action-specific information, as indicated by the low cosine similarities between weights for HOI classes associated with the action "ride". This suggests that shared information specific to the action "ride" is not well captured. Moreover, the weights for classes involving

the same object, "bike", show high similarity between each other, before weight adaptation. This demonstrates that in the original VLM feature space, actions linked to the same object tend to cluster together. After our proposed weight adaptation, the weight subset $\mathbf{W_{ar}}$ show noticeably higher similarities among classes that share the "ride" action.

C.4. Qualitative Results

We visualize our method's predictions across four settings in zero-shot HOI detection of HICO-DET: the unseen-verb setting in Fig. 9, the rare-first unseen-composition setting in Fig. 10, the non-rare-first unseen-composition setting in Fig. 11 and the unseen-object setting in Fig. 12. Our HOLa successfully identifies unseen HOI classes in various scenarios, demonstrating its generalization ability to unseen HOI classes. This performance is due to our low-rank decomposed feature adaptation that emphasizes class-shared information, thereby enhancing generalization to unseen classes. Additionally, the incorporation of action priors helps reduce overfitting to seen classes.

C.5. Controlability

While the learned basis features in our low-rank decomposition is not directly interpretable, our method enhances controllability by restricting adaptation to a low-dimensional subspace, spanned by basis vectors $\mathbf{b}_i \in \mathbf{B}$. In this subspace, explicit structures (e.g., orthogonality) are enforced and inspected, instead of modifying the features in the full VLM space.

C.6. Limitations

While our method achieves strong performance in zero-shot HOI detection, it relies on predefined unseen HOI class names, a standard requirement in zero-shot protocols [14–16, 39, 50]. However, this dependency limits flexibility and scalability in real-world scenarios where such predefined



Figure 10. Visualization of HOI predictions in the rare-first unseen-composition setting on HICO-DET. The purple bar indicates predictions for seen HOI classes and the yellow bar indicates predictions for unseen HOI classes.



Figure 11. Visualization of HOI predictions in the non-rare-first unseen-composition setting on HICO-DET. The purple bar indicates predictions for seen HOI classes and the yellow bar indicates predictions for unseen HOI classes.



Figure 12. Visualization of HOI predictions in the unseen-object setting on HICO-DET. The purple bar indicates predictions for seen HOI classes and the yellow bar indicates predictions for unseen HOI classes.

classes may be unavailable. To address this, our future work will focus on extending our approach to open-vocabulary

HOI detection [25, 53].

C.7. Future Work Exploration

In our method, adaptation with low-rank decomposition is applied to the language branch, specifically on action and interaction features, to enhance generalization to unseen classes. This design leverages the availability of unseen class text descriptions during training, enabling the model to incorporate class-shared knowledge from both seen and unseen HOI classes.

Similar techniques could potentially be extended to object features in the language branch or to visual features. However, in standard two-stage HOI methods [14, 15, 24], object detection is typically handled by an off-the-shelf detector. As a result, the primary challenge in HOI detection lies in modeling unseen actions or novel action-object pairs, rather than object categories, where object generalization is addressed separately in open-vocabulary object detection. However, applying low-rank decomposition to object features may offer a promising direction to benefit open-vocabulary object detection as well.

Furthermore, visual features from unseen classes are not accessible under the standard zero-shot setting, making it infeasible to inject unseen information into the vision branch during training. Exploring decomposition strategies in the vision branch under settings with full or partial visual supervision is another promising avenue for future work.